Available online at www.sciencedirect.com
ScienceDirect
Journal of Molecular Catalysis A: Chemical 260 (2006) 255–263
JOURNAL OF MOLECULAR CATALYSIS A: CHEMICAL
www.elsevier.com/locate/molcata

Study of an iron-based Fischer–Tropsch synthesis catalyst incorporated with SiO_2

Hai-Jun Wan [a,b], Bao-Shan Wu [a], Zhi-Chao Tao [a,b], Ting-Zhen Li [a,b], Xia An [a,b], Hong-Wei Xiang [a], Yong-Wang Li [a,*]

[a] *State Key Laboratory of Coal Conversion, Institute of Coal Chemistry, Chinese Academy of Sciences, Taiyuan 030001, People's Republic of China*
[b] *Graduate School of Chinese Academy of Sciences, Beijing 100039, People's Republic of China*

Received 25 May 2006; received in revised form 23 July 2006; accepted 24 July 2006
Available online 1 September 2006

Abstract

The effect of adding SiO_2 to a precipitated iron-based Fischer–Tropsch synthesis (FTS) catalyst was investigated using N_2 physical adsorption, H_2 differential thermogravimetric analysis, temperature-programmed reduction/desorption (TPR/TPD) and Mössbauer spectroscopy. The FTS performances of the catalysts with or without SiO_2 were compared in a fixed bed reactor. The characterization results indicated that SiO_2 facilitates the high dispersion of Fe_2O_3 and significantly influences the Fe/Cu and Fe/K contacts, which play an important role in the surface basicity, reduction and carburization behaviors, as well as the FTS performances. The incorporation of SiO_2 enhances the Fe/Cu contact, further enlarges the H_2 adsorption and promotes the reduction of $Fe_2O_3 \rightarrow FeO_x$, while the transformation of $FeO_x \rightarrow Fe$ is suppressed probably due to the strong Fe–SiO_2 interaction. SiO_2 indirectly weakens the surface basicity and severely suppresses the carburization and CO adsorption of the catalyst. In the FTS reaction, it was found that SiO_2 decreases the FTS initial activity but improves the catalyst stability. Due to the lower surface basicity than the catalyst without SiO_2, the catalyst incorporated with SiO_2 has higher selectivity to light hydrocarbons and methane and decreased selectivity to the olefins and heavy hydrocarbons.

Keywords: Fischer–Tropsch synthesis; Iron-based catalyst; SiO_2; Fe–SiO_2 interaction

1. Introduction

Fischer–Tropsch synthesis (FTS) has been industrialized in SASOL for almost fifty years and proved to be a promising route to meet the continuously increasing demand for liquid fuels [1,2]. Due to the excellent water gas shift reaction activity, the use of iron-based catalyst has attracted much attention for FTS with low H_2/CO ratio synthesis gas from coal gasification [3,4]. In order to obtain excellent performances of iron-based catalyst, a lot of attempts have focused on the addition of chemical promoters such as K_2O and CuO as well as structural promoters, including SiO_2, Al_2O_3, ZnO, MgO and TiO_2 [5,6]. Chemical promoters have been always thought to facilitate the reduction of the catalyst as well as the adsorption and dissociation of CO, while the structural promoters serve the purpose of improving the attrition resistance and stability [7–10]. SiO_2, Al_2O_3 and TiO_2 have been extensively investigated as structural promoters [11,12]. SiO_2 was found to be the most preferable one in terms of both activity and selectivity [13,14]. Especially in recent years, SiO_2 was chosen as the principal structural promoter for the preparation of iron-based catalysts with high attrition resistance using co-precipitated method and popular spray-drying technology. However, catalysts containing SiO_2 usually suffer from lower FTS activity in the FTS reaction. Therefore, a large number of studies were carried out to investigate the relationship between SiO_2 and FTS performances. Jun et al. [15] studied FTS over SiO_2 supported iron-based catalysts from biomass-derived syngas. They found that the addition of SiO_2 leads to the poor dispersion of iron oxide, inhibits the interaction between Fe and Cu, suppresses the reduction of $Fe_2O_3 \rightarrow Fe_3O_4$, decreases the FTS activity and enhances the selectivity to gaseous hydrocarbons. Recently, Yang et al. [13] investigated the impact of SiO_2 content on the reduction and catalytic performances over precipitated Fe–Mn catalyst prepared

* Corresponding author. Tel.: +86 351 4130337; fax: +86 351 4050320.
E-mail addresses: ywl@sxicc.ac.cn, haijunwan@163.com (Y.-W. Li).

1381-1169/$ – see front matter © 2006 Elsevier B.V. All rights reserved.
doi:10.1016/j.molcata.2006.07.062

by normal-dried. The results showed that a certain amount of SiO_2 incorporated into Fe–Mn catalyst decreases the catalyst crystallite size, favors the reduction of $Fe_2O_3 \rightarrow FeO$, enhances the selectivity to heavy hydrocarbons and improves the catalyst stability. Although SiO_2 as structural promoter has been widely used and investigated, the effects of SiO_2 on the iron-based catalyst still keep some inconsistent conclusions, because these studies were conducted under different conditions or over different catalyst systems. Thus, there are still unabated attempts for further investigation to understand the factors what SiO_2 affects the activity, selectivity and stability of iron-based catalyst.

On iron-based catalyst incorporated with SiO_2, the existence of Fe–SiO_2 interaction has been extensively discussed in literature [6,14,16]. However, little attention is focused on the effect of SiO_2 on the contacts between iron and chemical promoters, especially for multicomponent catalysts. It is well known that the intimate contacts between iron and chemical promoters result in an important influence on the catalyst activity and selectivity [4,6,15]. Many techniques, such as SEM, TEM, XRD and XPS failed to characterize its effect on the iron-promoters contacts. Temperature-programmed reduction (TPR) is a useful method for studying this effect, and temperature-programmed desorption (TPD) can further confirm the results. However, in previous reports [4,6,14,16], little information about the effect of SiO_2 on the iron-promoters contacts was provided by TPR and TPD.

The present study is undertaken to investigate the effect of SiO_2 on the contacts of Fe/Cu and Fe/K, as well as FTS performances. Several characterization methods, such as H_2-DTG, TPD (H_2, CO_2 and CO) and second run H_2-TPR are used together to characterize the iron-promoters contacts and to illustrate the function of SiO_2 in the catalyst. In addition, CO-TPR and Mössbauer spectroscopy are used to explain the effect of SiO_2 on the reduction, carburization and FTS performances.

2. Experimental

2.1. Catalyst synthesis procedure

Two catalysts used in this study were prepared by a combination of co-precipitated and spray-dried method. The detailed preparation method has been described elsewhere [16–18]. In brief, a solution containing both $Fe(NO_3)_3$ and $Cu(NO_3)_2$ with a weight ratio of 100Fe/6Cu was precipitated at 80 °C using Na_2CO_3 solution. After precipitation and filtration, the precipitate was divided into two parts: one of them was added with K_2CO_3 solution and silica gel in the amounts required to obtain the desired weight ratio of 100Fe/5K/25SiO_2. The other part of precipitate was only added with the appropriate amount of K_2CO_3 solution to obtain an unsupported iron-based catalyst. The slurry was spray dried and then was calcined at 450 °C for 5 h. The calcined catalyst was crushed and sieved to obtain 20–40 mesh for reaction. The final obtained catalysts were composed of 100Fe/5.9Cu/4.6K/28·7SiO_2 and 100Fe/5.7Cu/4.6K in mass ratio. These two catalysts were labeled as Si-25 and Si-0, respectively.

2.2. Reactor system and pretreatment procedures

The experiments were conducted in a 12 mm i.d. stainless steel fixed bed reactor. For all reaction experiments, 5 ml catalyst was mounted in the reactor and was activated using synthesis gas ($H_2/CO = 2.0$) at 280 °C, 0.1 MPa and 1000 h^{-1} for 18 h. After reduction, Fischer–Tropsch synthesis reaction was carried out at conditions of 260 °C, 2.0 MPa, $H_2/CO = 2.0$ and GHSV = 1000 h^{-1} over a period of 230 h steady-state runs. During the mass balance period (generally 24 h), the tail gas was analyzed on several off-line gas chromatographs (GC). H_2, CO and CH_4 were analyzed on a GC 920 (Shanghai Analyzer Co., People Republic of China) with a thermal conductivity detector (TCD). The amount of CO_2 in tail gas was determined on a GC 920 and TCD. C_1–C_8 hydrocarbons were analyzed on a Shimadzu-7A GC and a flame ionization detector (FID). The analysis of the oil product was performed on an Agilent 6890N (HP) GC with DB-1 quartz capillary column (FID, N_2 carrier). The heavy wax was analyzed using a GC920 with UA^+-(HT) stainless steel capillary column (FID, N_2 carrier).

2.3. Catalyst characterization equipments and procedures

The composition of the catalysts was determined by atomic adsorption spectropy (AAS) using an Atomscan 16 spectrometer (TJA, USA).

The BET surface area, pore volume and average pore size were measured by N_2 physical adsorption at −196 °C using a Micromeritics ASAP 2500 instruments. The samples were degassed under vacuum at 180 °C for 6 h before measurement.

The H_2-DTG was carried out by thermal gravimetric (TG) using an MS OmniStar 200 instrument. About 20–30 mg of catalyst was treated in 5% H_2/95% Ar (v/v) (flow rate of 50 ml/min) and the reduction temperature was increased from room temperature to 800 °C at a heating rate of 10 °C/min.

The second run H_2-TPR and CO-TPR were performed in a quartz reactor using 5% H_2/95% Ar (v/v) or 5% CO/95% He (v/v) as the reactant. The H_2 or CO consumption was monitored by the change of thermal conductivity of the effluent gas stream. Typically, about 20 mg catalyst was packed in the quartz reactor and the flow rate of the reduction gas was 100 ml/min in the standard state. The reduction temperature in the second run TPR was increased to 450 °C at a heating rate of 6 °C/min and kept at 450 °C for 1 h. After the first H_2-TPR, the sample was purged with Ar, cooled to room temperature, and then reoxidized by temperature-programmed oxidization in 5% O_2/95% He (v/v) with the same temperature program used in the first run (temperature increased to 450 °C at a heating rate of 6 °C/min and kept at 450 °C for 1 h). The second run TPR was then performed for the reoxidized catalyst sample. In the CO-TPR, the reduction temperature was increased from room temperature to 800 °C and a liquefied nitrogen bath was used to remove CO_2 formed during the carbon monoxide reduction.

The H_2, CO or CO_2-TPD experiments were performed in the same system as used in CO-TPR with Ar (in H_2-TPD) or He (in CO-TPD or CO_2-TPD) as carrier gas. About 200 mg sample was loaded in the reactor. It must be noted specially that, for the H_2

Table 1
Textural properties of the catalyst samples as prepared

Catalyst	BET surface area (m^2/g)	Pore volume (cm^3/g)	Average pore size (nm)
Si-0	20	0.14	28.43
Si-25	161	0.20	5.11

or CO-TPD experiments, the catalyst was first reduced with H_2 at 450 °C or CO at 300 °C for 4 h. In the CO_2-TPD experiments, the catalyst sample was purged with He (50 ml/min) and calcined in situ to remove the adsorption species from the catalysts. In the following steps, H_2, CO or CO_2 adsorption on catalyst was performed at 100 °C for 30 min, and then the sample was purged with the carrier gas for 30 min to remove the weakly adsorbed species. After this step, the TPD was carried out.

The Mössbauer spectra of catalysts were recorded at room temperature using a CANBERRA Series 40 MCA constant-acceleration Mössbauer spectrometer (CANBERRA, USA), using a 25 mCi ^{57}Co in Pd matrix. The spectrometer was operated in the symmetric constant acceleration mode. The spectra were collected over 512 channels in mirror image format. Data analysis was performed using a nonlinear least squares fitting routine that models the spectra as a combination of singlets, quadruple doublets and magnetic sextuplets based on a Lorentzian line shape profile. The spectral components were identified based on their isomer shift (δ), quadruple splitting (Δ) and magnetic hyperfine field (Hhf). All isomer shift values were reported with respect to metallic iron (α-Fe) at the measurement temperature. Magnetic hyperfine fields were calibrated with the 330 kOe field of α-Fe at ambient temperature.

The reduced catalysts used for Mössbauer spectroscopy were obtained by reducing the catalyst samples in a quartz reactor with synthesis gas (H_2/CO = 2.0) at 280 °C, 0.1 MPa and 1000 h^{-1} for 18 h. After reduction, the quartz reactor was sealed and transferred to a glove box. Under the Ar atmosphere, the reduced catalysts were transferred to a glass vial and coated with liquid paraffin for further characterization test.

3. Results and discussion

3.1. Textural properties

The surface area and pore size distribution of the fresh catalysts are listed in Table 1 and Fig. 1, respectively. It is apparent that SiO_2 significantly influences the surface area, pore volume and pore size distribution. Incorporated with SiO_2, catalyst Si-25 has large surface area and pore volume and small pore size. It is probably that incorporation of SiO_2 into the porous precipitate provides a rigid matrix, which helps to prevent the catalyst from fast pore collapse and stabilize the small iron oxide crystallites from sintering during the high-temperature calcination process [15]. The large surface area is hence due to the small catalyst crystallites. The MES results in the present study also show that the catalyst incorporated with SiO_2 has smaller catalyst crystallite than the catalyst without SiO_2.

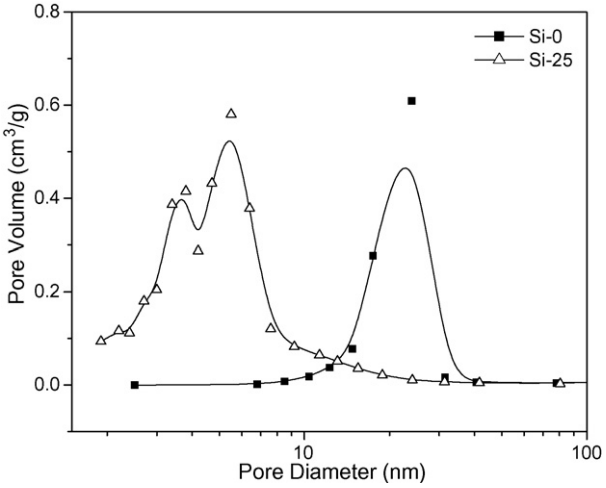

Fig. 1. The pore size distribution of the catalyst samples.

3.2. H_2-DTG and second run H_2-TPR

H_2-DTG was used to investigate the effect of SiO_2 on the reduction behavior of the catalyst. As shown in Fig. 2, the reduction process of the two catalysts occurs in two distinct stages. For catalyst Si-25, the reduction starts at lower temperature and finishes at higher temperature as compared with that of catalyst Si-0. The quantitative results from weight loss measurements during different reduction stages are summarized in Table 2. The experimental weight loss of the first stage for catalyst Si-0 is consistent with the corresponding theoretical weight loss based on the process of $CuO \rightarrow Cu$ and $Fe_2O_3 \rightarrow Fe_3O_4$, and the second stage corresponds to the transformation of $Fe_3O_4 \rightarrow Fe$. The first stage can be further separated into two peaks, the small peak at lower temperature is ascribed to the transformation of $CuO \rightarrow Cu$ and the large peak at higher temperature represents the transformation of $Fe_2O_3 \rightarrow Fe_3O_4$. The result implies that partial CuO and the iron oxides phases could remain segregated; hence the reduction peak of the first stage shifts to higher temperature as compared with catalyst Si-25. As shown in Table 2, the experimental weight loss of the first stage for catalyst Si-25 is larger than the theoretical amount corresponding to the transformation of $CuO \rightarrow Cu$ and $Fe_2O_3 \rightarrow Fe_3O_4$, but it is lower than

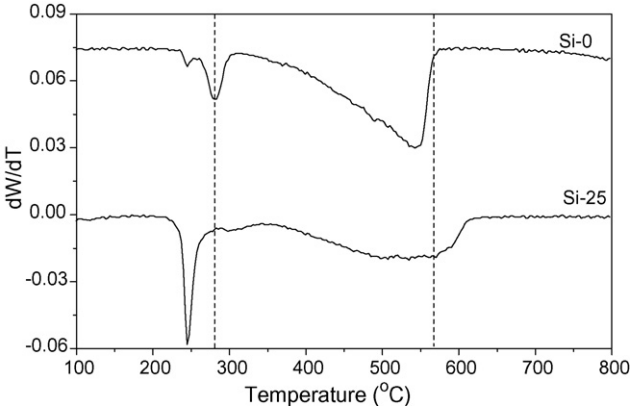

Fig. 2. H_2-DTG profiles of the catalysts.

Table 2
Theoretical and experimental weight loss of the catalysts

Catalyst	Catalyst weight as-loaded (mg)	Theoretical weight loss (mg)			Experimental weight loss (mg)	
		$Fe_2O_3 \rightarrow Fe_3O_4$ CuO → Cu	$Fe_2O_3 \rightarrow$ FeO CuO → Cu	$Fe_2O_3 \rightarrow$ Fe CuO → Cu	First stage	Total
Si-0	21.45	0.75	2.16	6.08	0.75	6.06
Si-25	22.19	0.75	1.88	5.32	1.44	5.07

those of CuO → Cu and $Fe_2O_3 \rightarrow$ FeO. It is confirmed that partial Fe_2O_3 may be converted to FeO with incorporation of SiO_2 in the first stage. Therefore, the first stage of catalyst Si-25 is attributed to the transformations of CuO → Cu, $Fe_2O_3 \rightarrow Fe_3O_4$ and $Fe_3O_4 \rightarrow$ FeO and the second stage of the catalyst corresponds to the transformations of $Fe_3O_4 \rightarrow$ Fe and FeO → Fe. Total experimental weight loss of catalyst Si-0 is consistent with the theoretical value based on the process of CuO → Cu and $Fe_2O_3 \rightarrow$ Fe within experimental errors, but the total experimental value of Si-25 is lower than the total theoretical value. Such a result implies that catalyst Si-0 is completely reduced to Fe, whereas catalyst Si-25 is partially reduced in H_2 atmosphere under 800 °C.

The H_2-DTG clearly shows that the incorporation of SiO_2 promotes the reduction of the first stage, but it suppresses the reduction of the second stage. The probably reason is that the addition of SiO_2 facilitates the high dispersion of Fe_2O_3 and CuO as demonstrated by MES in the later section, and could further enhance the Fe/Cu contact, resulting in the reduction temperature of the first stage shifting to lower temperature. On the other hand, a certain amount of SiO_2 incorporated into the iron-based catalyst decreases the crystallite size of Fe_2O_3, which also favors the reduction of Fe_2O_3 [13]. However, the second stage of Si-25 finishes at higher temperature, implying that the addition of SiO_2 suppresses the reduction of $Fe_3O_4 \rightarrow$ Fe and FeO → Fe. FeO is a metastable phase of iron oxides blow 570 °C [19]. Previous studies have proposed that FeO phase is stabilized on the support, while no such phase is seen in unsupported catalyst [20–22]. This result is consistent with that only Fe_3O_4 exists on catalyst Si-0, while Fe_3O_4 and FeO coexist on catalyst Si-25 at the first stage. Quantitative results from weight loss measurement show that small amount of FeO could still exist on catalyst Si-25 after TPR run. The appearance of FeO phase may be stable on SiO_2 due to the strong Fe–SiO_2 interaction [23], which suppresses the reduction of FeO → Fe and results in the reduction peak shifting to higher temperature.

The H_2-DTG results provide evidence that the addition of SiO_2 enhanced the contact between Fe_2O_3 and CuO. The second run H_2-TPR further confirms this function of SiO_2. As showed in Fig. 3, all profiles of the two catalysts present two reduction peaks, indicating that the reduction process occurs in two distinct stages. For catalyst Si-0, the first reduction peak shifts to higher temperature and the second reduction peak shows a larger reduction area in higher temperature in the second run

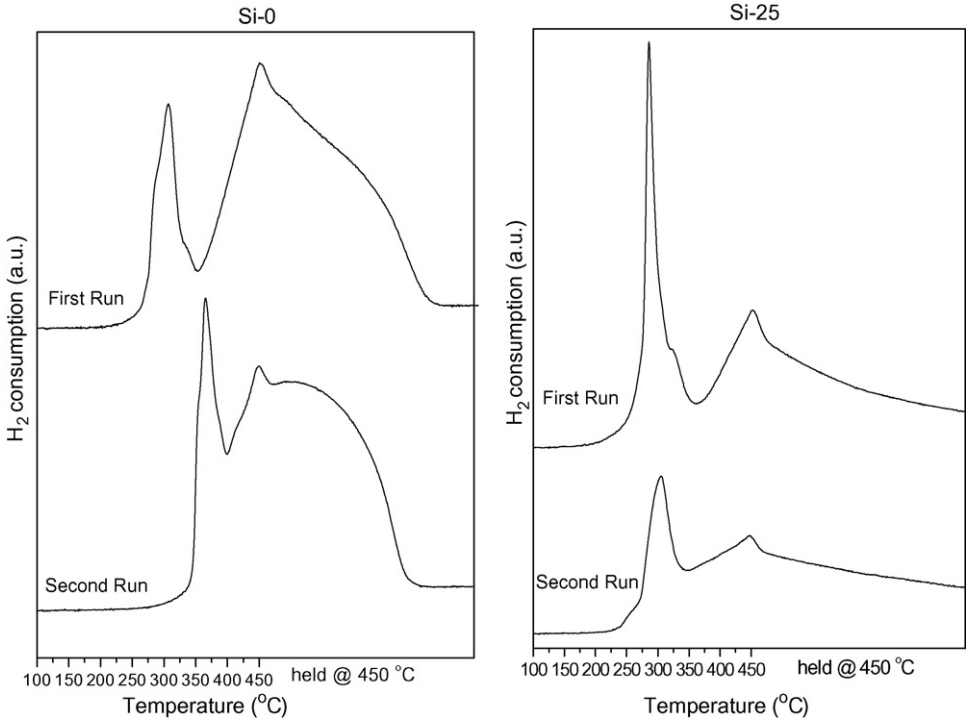

Fig. 3. Second run H_2-TPR profiles for the two catalysts.

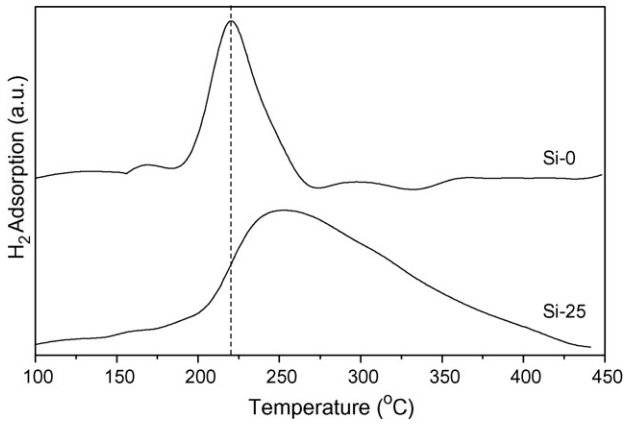

Fig. 4. H_2-TPD profiles of the two catalysts.

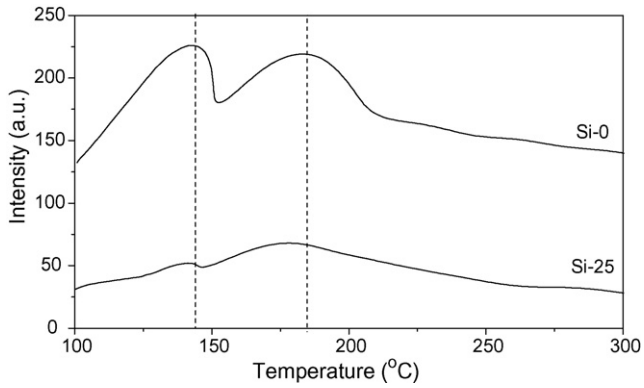

Fig. 5. CO_2-TPD profiles for the two catalysts.

compared with the first run, indicating that the catalyst without SiO_2 is more difficult to be reduced after the first run and reoxidation [4]. For the catalyst incorporated with SiO_2, in the second run the location of all reduction peaks do not change apparently as compared with the first run, whereas the first peak is broader and the second reduction peak becomes difficultly to go back to the baseline. The result can be reasoned that the Fe–SiO_2 interaction could be enhanced after the first run and reoxidation and further suppresses the reduction of the second stage ($FeO_x \rightarrow Fe$).

The second run H_2-TPR clearly shows that, when the catalyst without SiO_2 was subjected to 450 °C oxidation after the first run TPR and a second run TPR was performed, the first peak apparently shifts to high temperature. Jin and Datye [4] reported that the major differences between the first and second TPR runs can be related to the segregation of Fe_2O_3 and CuO phases. It seems that CuO to serve as a promoter, the intimate contact with iron oxide is essential. The catalyst without SiO_2 could easily sinter and lead to the further segregation of Fe_2O_3 and CuO phases during the high-temperature reduction in the first run and reoxidation; therefore, the second run is very different from the first one. As the result of textural properties shown, the addition of SiO_2 is very effective at inhibiting the sintering of catalyst crystallites, and could prevent the segregation of Fe_2O_3 and CuO phases after the first run and reoxidation. Thus, a comparison of the first run H_2-TPR and the second run H_2-TPR shows that catalyst Si-25 keeps the unchanged reduction temperature.

3.3. H_2-TPD

Fig. 4 shows the adsorption behavior of H_2 from catalysts with or without SiO_2. All of the H_2-TPD profiles have only one peak, indicating that only one type of adsorbing species could exist over the catalysts. The desorption temperature and amount desorbed from Si-25 both are higher than those measured for Si-0. Clearly, the addition of SiO_2 not only leads to the large amount of H_2 adsorption, but also shifts the adsorption peak to higher temperature. Previous studies [23,24] over iron catalysts have indicated that the incorporation of CuO into iron-based catalyst enlarges the adsorption amount of H_2 and further facilitates the reduction of iron-based catalyst. The results of H_2-TPD in present study are attributed to that the incorporation of SiO_2 into the catalyst enhances the contact between Fe_2O_3 and CuO, which could strengthen the ability of H_2 adsorption. This result further confirms the observed in H_2-DTG and second run H_2-TPR.

3.4. Surface basicity

CO_2-TPD is used to investigate the effect of SiO_2 on the surface basicity of the catalysts [25,26], and these profiles are present in Fig. 5. It shows clearly that all catalysts have two groups of desorption peaks; one at the lower temperatures corresponding to weak CO_2 adsorption, while the other at higher temperatures is ascribed to strong CO_2 adsorption. Apparently, the catalyst incorporated with SiO_2 has weaker CO_2 adsorption than the catalyst without SiO_2, indicating that SiO_2 as structural promoter weakens the surface basicity.

The studies of Zhang et al. [23] over Fe–Mn catalyst revealed that K plays a critical role in improving the surface basicity. They also mentioned that the strong interaction between K and SiO_2 significantly reduced the amounts of total basic sites. The analysis of CO_2-TPD reveals that the weakened surface basicity of the catalyst incorporated with SiO_2 can be directly correlated with the effective potassium content. Dry and Oosthuizen [27] reported that more K was required when acidic compounds, e.g., SiO_2 were present. In other words, K interacts so severely with SiO_2 as to decrease the content of effective potassium. The possible reason is that, during the preparation of the catalyst, the acidic SiO_2 will combine with the basic K promoter, forming the strong K–SiO_2 interaction. This interaction could weaken the intimate contact between Fe_2O_3 and K, and further decreases the surface basic sites. On the other hand, as stated in H_2-DTG, the stronger Fe–SiO_2 interaction existing on catalyst Si-25 could also weaken the Fe/K contact [13]. As a consequence, the weakened promotional effect of potassium decreases the surface basic sites.

3.5. CO-TPR and CO-TPD

The carburization behavior of the catalysts is studied by CO-TPR. The CO-TPR patterns are shown in Fig. 6. The changes in shape of these curves suggest that SiO_2 strongly

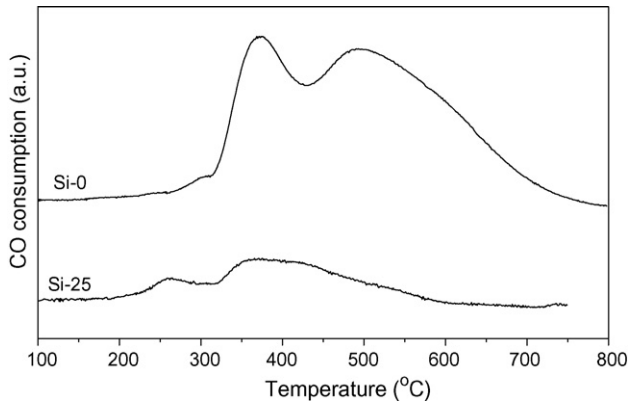

Fig. 6. CO-TPR profiles of the catalysts.

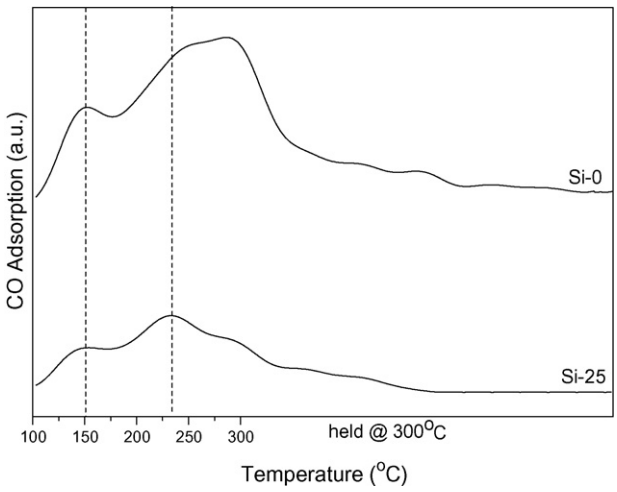

Fig. 7. CO-TPD profiles of the two catalysts.

affects the carburization of the catalyst. For catalyst Si-0, the reduction peak at 291 °C is attributed to the transformation of $Fe_2O_3 \rightarrow Fe_3O_4$, while the two high-temperature peaks in the range of 300–750 °C are attributed to the carburization of the catalyst. A sharp decrease in the rate of CO consumption occurs at 430 °C, indicating that the carburization process could occur in two stages. According to the literature [4], the first stage corresponds to the transformation of Fe_3O_4 to iron carbide, while the second stage is attributed to carbon deposition. For catalyst Si-25, the catalyst is reduced and carburized via two steps. It is clearly shown that the incorporation of SiO_2 promotes the reduction of $Fe_2O_3 \rightarrow Fe_3O_4$ and leads to the transformation of $Fe_2O_3 \rightarrow Fe_3O_4$ shifting to lower temperature. The result is consistent with the observed in H_2-DTG (Fig. 2). However, compared with catalyst Si-0, the addition of SiO_2 significantly suppresses the carburization and carbon deposition. The result of CO_2-TPD has indicated that the effective potassium content of catalyst Si-25 is seriously reduced by the addition of SiO_2. Therefore, the weakened promotional effect of potassium leads to the weak carburization and suppresses carbon deposition.

CO-TPD is used to investigate the effect of SiO_2 on the CO adsorption. As shown in Fig. 7, all catalysts have two groups of desorption peaks; one at the lower temperatures corresponding to the weak CO adsorption, while the other at higher temperatures is ascribed to the strong CO adsorption. It is interesting to note that the strong desorption peak shifts to lower temperature and the two desorption peaks are weakened with the addition of SiO_2, indicating that SiO_2 as structural promoter will suppress the CO adsorption strongly. Miller and Moskovits [28] reported that as the K level increases, the extent of adsorption CO is significantly increased. In other words, K plays an important role in the CO adsorption for iron-based catalyst. The studies of Dry indicated that the weak surface basicity of iron-based catalyst can suppress the adsorption of CO [27]. Reviewing the CO_2 adsorption in previous section of this paper, a clear relationship between SiO_2 and the ability of CO adsorption is exhibited; the incorporation of SiO_2 into the catalyst weakens the Fe/K contact, decreases the surface basic sites and further leads to weak CO adsorption.

3.6. Bulk phase structure of the catalysts

The phase composition of the catalysts is determined by MES analyses. Fig. 8 shows the Mössbauer spectra of the catalysts before and after reduction and after reaction. Table 3 lists the iron-phase composition of the catalysts, as determined by fitting the Mössbauer spectra. For the fresh catalyst samples, the content of superparamagnetic Fe^{3+} ions of catalyst Si-25 is higher than that of catalyst Si-0, indicating that the catalyst crystallite size of Si-25 is smaller. Such a result in combination with the BET surface area data indicates that the addition of SiO_2

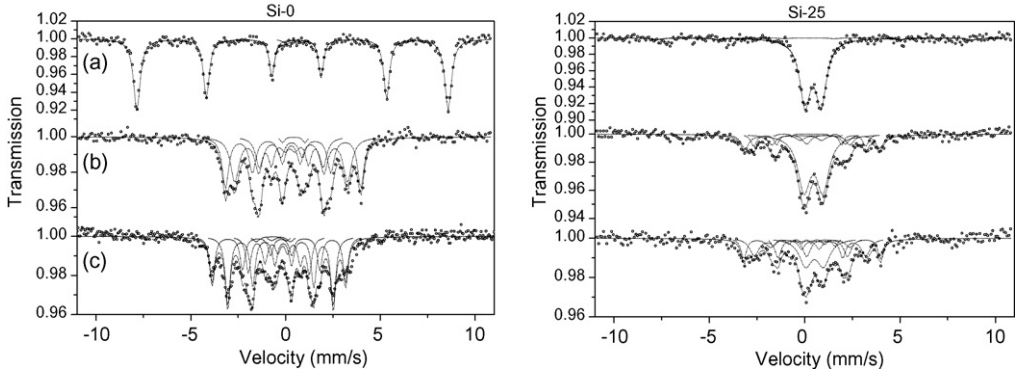

Fig. 8. Mössbauer spectra of catalysts Si-0 and Si-25 at different states: (a) as prepared, (b) after reduction and, (c) reaction for 230 h.

Table 3
Iron phase composition of the catalysts at different states

Catalysts	Si-0		Si-25	
	Phase	Area (%)	Phase	Area (%)
Oxide	α-Fe_2O_3	97.5	α-Fe_2O_3	5.1
	Fe^{3+}	2.5	Fe^{3+}	94.9
After reduction	FeC_x	98.2	FeC_x	35.8
	Fe^{3+}	1.3	Fe^{3+}	56.8
	Fe^{2+}	0.5	Fe^{2+}	7.4
Reaction for 230 h	Fe_3O_4 (A)	0.3	Fe_3O_4 (A)	0
	Fe_3O_4 (B)	1.4	Fe_3O_4 (B)	0
	FeC_x	98.3	FeC_x	58.3
	Fe^{3+}	0	Fe^{3+}	29.1
	Fe^{2+}	0	Fe^{2+}	12.6

suppresses the enlargement of the crystallites size of α-Fe_2O_3 during the high-temperature calcination process. After reduced in synthesis gas, catalyst Si-0 has much more iron carbides and less superparamagnetic Fe^{3+} ions than Si-25. It implies that the addition of SiO_2 might weaken the promotional effect of potassium and seriously suppresses the carburization of the catalyst due to strong K-SiO_2 and Fe–SiO_2 interactions. The result is in good agreement with CO-TPR. As shown in Table 3 and Fig. 8, the extent of carburization on catalyst Si-0 after reaction for 230 h is similar to that after reduced, whereas superparamagnetic Fe^{3+} and Fe^{2+} ions completely disappears and little amount of Fe_3O_4 appears. For catalyst Si-25, although the content of iron carbides increases after reaction for 230 h, there are still large amounts of superparamagnetic Fe^{3+} and Fe^{2+} ions as compared with that of Si-0, implying that catalyst Si-25 has smaller particle size than catalyst Si-0.

3.7. FTS performances

Fischer–Tropsch synthesis performances of the two catalysts were measured at reaction conditions of 260 °C, 1.5 MPa, 1000 h^{-1} and $H_2/CO = 2.0$. The activities, stabilities and product selectivities were tested over a period of 230 h steady-state runs.

3.7.1. Activity and stability

The effects of SiO_2 on CO conversion are shown in Fig. 9. Catalyst Si-0 has higher initial activity and deactivates quickly with time on stream, whereas the CO conversion of catalyst Si-25 is stable or even increases slowly. Apparently, incorporation of SiO_2 into the catalyst decreases the catalyst activity, but improves the catalyst stability. It is generally accepted that the iron carbides are main active phases for the FTS reaction [29–33]. Although the FTS reaction does not occur in the bulk phase of carbides, the carbides can have FTS active sites on their surfaces. Thus, the content of iron carbides determined by MES can be used to monitor the amount of FTS active sites to some extent. As stated in the MES results, the incorporation of SiO_2 seriously suppresses the carburization of the catalyst due to the weakened promotional effect of potassium. Numerous studies have shown that the ability of CO adsorption plays an important role in the FTS activity [16,23,27]. Recalling the results of CO-TPR and CO adsorption in the present study, the weakened carburization on catalyst incorporated with SiO_2 generates small amount of FTS active sites and could further suppress the adsorption of CO; hence catalyst Si-25 has lower activity. As the result of MES shown, catalyst Si-0 is easily carburized and could have large amount of FTS active sites, which could significantly enhance the adsorption of CO, and thus a higher initial activity is obtained.

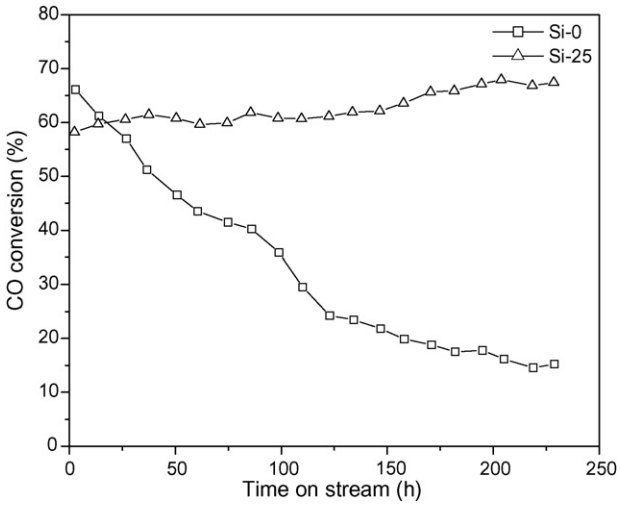

Fig. 9. The carbon monoxide conversion of the catalysts. Reaction condition: 260 °C, 2.0 MPa, $H_2/CO = 2.0$ and GHSV = 1000 h^{-1}.

As Fig. 9 shown, catalyst Si-0 deactivates quickly, whereas the CO conversion of the catalyst incorporated with SiO_2 is stable or even increases with time on stream. As indicated by CO-TPR, catalyst Si-0 is easily carburized and could accumulate more carbon during FTS reaction, which could cover large amount of FTS active sites and results in deactivation [34]. However, the addition of SiO_2 could suppress the carbon deposition during the reduction and reaction process, and further improves the stability of the catalyst. On the other hand, as the textural properties and MES results shown, the catalyst without SiO_2 could easily aggregate during high temperature FTS reaction and deactivates quickly, whereas the incorporation of SiO_2 into the iron-based catalyst could suppress the aggregation of the catalyst crystallites and maybe further improve the catalyst stability.

3.7.2. Product selectivity

Hydrocarbon product distribution of the two catalysts is shown in Table 4. It shows that the selectivities to gaseous and light hydrocarbons (methane, C_2–C_4 and C_5–C_{11}) are enhanced, whereas those to heavy hydrocarbons (C_{12}^+ and C_{19}^+) and olefins ($C_2^=$–$C_4^=$ and $C_5^=$–$C_{11}^=$) are suppressed with the incorporation of SiO_2 into the catalyst. All of these results imply that the chain growth reaction is restrained and the hydrogenation reaction is enhanced on the catalyst incorporated with SiO_2. It is well known that the weakened surface basicity of iron-based catalyst can suppress the dissociative adsorption of CO, retard the chain propagation reaction and reduce the selectivity of olefin

Table 4
Activity and selectivity of the two catalysts

Catalysts	Si-0		Si-25	
	86[a]	158[a]	86[a]	158[a]
CO conversion (%)	42.8	20.8	60.9	62.8
H_2 + CO conversion (%)	30.0	14.6	43.3	44.2
Exit molar H_2/CO ratio	2.71	2.24	2.88	2.82
Hydrocarbon selectivities (wt.%)				
CH_4	5.3	5.0	16.5	16.1
$C_{2–4}$	24.9	23.3	34.4	34.0
$C_{5–11}$	29.2	30.5	35.9	34.1
$C_{12–18}$	18.3	18.8	8.9	8.5
C_{19}^+	22.3	22.4	4.4	7.2
Olefin selectivity (wt.%)				
$C_2^=$–$C_4^=$	54.5	55.2	50.3	49.5
$C_5^=$–$C_{11}^=$	73.8	74.9	68.2	67.6

Reaction condition: 260 °C, 2.0 MPa, H_2/CO = 2.0 and GHSV = 1000 h^{-1}.
[a] Time on stream (h)

[25,28,35]. The results obtained in the present study indicate that the addition of SiO_2 obviously decreases the surface basicity and further suppresses the CO adsorption. Thus, the FTS selectivity results reconfirmed that the surface basic sites existing on catalyst Si-25 are responsible for the enhancement of the gaseous hydrocarbons and light hydrocarbon product and the suppression of heavy products and olefins. The weak basic sites on the surface of Si-25 do not facilitate the CO dissociative adsorption, leading to a lower coverage of carbon species on the surface, whereas sufficient H_2 is present for chain termination rates and the light paraffin production due to the Fe/Cu contact enhanced indirectly by the incorporation of SiO_2.

4. Conclusions

Incorporation of SiO_2 to precipitated iron-based catalyst was found to have significant influences on the surface basicity, reduction and carburization behaviors, as well as catalytic activity. The changes in the catalytic performances can be primarily attributed to the effects of SiO_2 on the Fe/Cu and Fe/K contacts, which lead to different degrees of H_2 and CO adsorption and further significantly affect the FTS performances of the catalyst.

SiO_2 stabilizes the iron oxide crystallites from sintering, facilitates the high dispersion of Fe_2O_3 and CuO and further enhances the contact between Fe_2O_3 and CuO. The enhanced Fe/Cu contact enhances the ability of H_2 adsorption and promotes the reduction of $Fe_2O_3 \rightarrow FeO_x$, while the transformation of $FeO_x \rightarrow$ Fe is suppressed due to the stronger Fe–SiO_2 interaction. Furthermore, due to the strong Fe–SiO_2 and K–SiO_2 interactions, catalyst incorporated with SiO_2 has weak contact between Fe and K, which weakens the surface basicity of the catalyst and severely suppresses the carburization, resulting in the weak CO adsorption.

In the FTS reaction, the FTS activity is decreased by the addition of SiO_2 due to the weak carburization, whereas SiO_2 could suppress carbon deposition and thus improves the catalyst stability. With incorporation of SiO_2, the hydrocarbon selectivity was strongly affected. The product distribution shifts to the light hydrocarbons and the olefin selectivity in total product decreases on the catalyst due to the surface basicity weakened indirectly by the addition of SiO_2.

Acknowledgements

We deeply appreciate the financial support from the Chinese Academy of Sciences (Project No. KGCX1-SW-02), 863 Project of Ministry of Science and Technology of China (2001AA523010), and National Natural Science Foundation of China (20590361), respectively.

References

[1] V.S. Rao, G.J. Stiegel, G.J. Cinquergrane, R.D. Srivastava, Fuel Process. Technol. 30 (1992) 83.
[2] R.B. Anderson, The Fischer–Tropsch Synthesis, Academic Press, Orlando, FL, 1984.
[3] K. Jothimurugesan, J.G. Goodwin, S.K. Santosh, J.J. Spivey, Catal. Today 58 (2000) 335.
[4] Y. Jin, A.K. Datye, J. Catal. 196 (2000) 8.
[5] N. Egiebor, W.C. Cooper, Can. J. Chem. Eng. 63 (1985) 81.
[6] D.B. Bukur, X. Lang, D. Mukesh, W.H. Zimmerman, M.P. Rosynek, C. Li, Ind. Eng. Chem. Res. 29 (1990) 1588.
[7] M.A. Vannice, R.L. Garten, J. Catal. 66 (1980) 242.
[8] H.J. Jung, P.L. Walker, M.A. Vannice, J. Catal. 75 (1982) 416.
[9] H.N. Pham, A. Viergutz, R. Gormley, A.K. Datye, Powder Technol. 110 (2000) 196.
[10] R. Zhao, J.G. Goodwin, K. Jothimurugesan Jr., S.K. Gangwal, J.J. Spivey, Ind. Eng. Chem. Res. 40 (2001) 1065.
[11] M.V. Cagnoli, S.G. Marchetti, N.G. Gallegos, A.M. Alvarez, R.C. Mercader, A.A. Yeramian, J. Catal. 123 (1990) 21.
[12] R.J. O'Brien, L. Xu, S. Bao, A. Raje, B.H. Davis, Appl. Cata. A: Gen. 196 (2000) 173.
[13] Y. Yang, H.-W. Xiang, L. Tian, H. Wang, C.-H. Zhang, Z.-C. Tao, Y.-Y. Xu, B. Zhong, Y.-W. Li, Appl. Cata. A: Gen. 284 (2005) 105.
[14] H. Dlamini, T. Motjope, G. Joorst, G. ter Stege, M. Mdleleni, Catal. Lett. 78 (2002) 1.
[15] K.W. Jun, H.S. Roh, K.S. Kim, J.S. Ryu, K.W. Lee, Appl. Catal. A: Gen. 259 (2004) 221.
[16] Y. Yang, H.W. Xiang, Y.Y. Xu, L. Bai, Y.W. Li, Appl. Catal. A: Gen. 266 (2004) 181.
[17] B. Wu, L. Bai, H. Xiang, Y.W. Li, Z. Zhang, B. Zhong, Fuel 83 (2004) 205.
[18] B. Wu, L. Tian, L. Bai, Z. Zhang, H. Xiang, Y.W. Li, Catal. Commun. 5 (2004) 253.
[19] J.O. Edstrom, J. Iron Steel Inst. 175 (1953) 289.
[20] M. Boudart, A. Delbouille, J.A. Dumesic, S. Khammouma, H. Topsøe, J. Catal. 37 (1975) 486.
[21] A.J.H.M. Kock, H.M. Fortuin, J.W. Geus, J. Catal. 96 (1985) 261.
[22] A.F.H. Wielers, A.J.H.M. Kock, C.E.C.A. Hop, J.W. Geus, A.M. van der Kraan, J. Catal. 117 (1989) 1.
[23] C.H. Zhang, Y. Yang, B.T. Teng, T.Z. Li, H.Y. Zheng, H.W. Xiang, Y.W. Li, J. Catal. 237 (2006) 405.
[24] C. Zhang, B. Teng, Y. Yang, Z. Tao, Q. Hao, H. Wan, F. Yi, B. Xu, H. Xiang, Y. Li, J. Mol. Cata. A 239 (2005) 15.
[25] X. Wang, G. Li, U.S. Ozkan, J. Mol. Catal. A 217 (2004) 219.
[26] C. Schild, A. Wokaun, A. Baiker, J. Mol. Catal. 67 (1990) 223.
[27] M.E. Dry, G.J. Oosthuizen, J. Catal. 11 (1968) 18.
[28] D.G. Miller, M. Moskovits, J. Phys. Chem 92 (1988) 6081.
[29] D.B. Buker, K. Okabe, M.P. Rosynek, C. Li, D. Wang, K.R.P.M. Rao, G.P. Huffman, J. Catal. 155 (1995) 353.
[30] T.R. Motjope, H.T. Dlamini, G.R. Hearne, N.J. Coville, Catal. Today 71 (2002) 335.

[31] L.D. Mansker, Y. Jin, D.B. Bukur, A.K. Datye, Appl. Catal. A: Gen. 186 (1999) 277.
[32] S. Li, S. Krisyhnamoorthy, A. Li, G.D. Meitzner, E. Iglesia, J. Catal. 206 (2002) 202.
[33] S. Li, G.D. Meitzner, E. Iglesia, J. Phys. Chem. B 105 (2001) 5743.
[34] M.E. Dry, T. Shingles, L.J. Boshoff, G.J. Oosthuizen, J. Catal. 15 (1969) 190.
[35] J.W. Niemantsverdriet, A.M. vander Kraan, W.L. van Dijk, H.S. vander Baan, J. Phys. Chem. 84 (1980) 3363.